

The effect of primordial black holes on 21 cm fluctuations

Hiroyuki Tashiro¹ and Naoshi Sugiyama^{2,3}

¹*Physics Department, Arizona State University, Tempe, AZ 85287, USA*

²*Department of Physics and Astrophysics & Kobayashi-Maskawa Institute for the Origin of Particles and the Universe, Nagoya University, Chikusa, Nagoya 464-8602, Japan*

³*Institute for the Physics and Mathematics of the Universe (IPMU), The University of Tokyo, Kashiwa, Chiba, 277-8568, Japan*

14 November 2018

ABSTRACT

The 21 cm signal produced by non-evaporating primordial black holes (PBHs) is investigated. X-ray photons emitted by the accretion to a PBH ionize and heat intergalactic medium (IGM) gas near a PBH. Using a simple analytic model, we show that this x-ray heating can produce an observable differential 21 cm brightness temperature. The region of the observable 21 cm brightness temperature can extend to 1–10 Mpc comoving distance from a PBH with depending on the PBH mass. The angular power spectrum of 21 cm fluctuations due to PBHs is also calculated. The peak position of the angular spectrum depends on the PBH mass, while the amplitude is independent. Comparing it with the angular power spectrum caused by primordial density fluctuations, it is found that both of them become comparable if $\Omega_{\text{PBH}} = 10^{-12}(M/10^3 M_{\odot})^{-0.2}$ at $z = 30$ and $10^{-13}(M/10^3 M_{\odot})^{-0.2}$ at $z = 20$ for the PBH mass from $10 M_{\odot}$ to $10^8 M_{\odot}$. Finally we find that the Square Kilometer Array can detect the signal due to PBHs up to $\Omega_{\text{PBH}} = 10^{-9}(M/10^3 M_{\odot})^{-0.2}$ at $z = 30$ and $10^{-10}(M/10^3 M_{\odot})^{-0.2}$ at $z = 20$ for PBHs with mass from $10^2 M_{\odot}$ to $10^8 M_{\odot}$.

Key words: cosmology: theory – large-scale structure of universe

1 INTRODUCTION

It is believed that primordial black holes (PBHs) formed in the early Universe (Carr & Hawking 1974; Carr 1975). Although there is no direct evidence of the existence of PBHs, PBHs are attracting attention as the way of constraining physics in the early Universe. In particular, one of the main generation mechanisms of PBHs is a gravitational collapse of an overdensity region at the horizon scale when the amplitude of overdensity exceeded a critical threshold. Therefore the resultant mass function and the abundance of PBHs depend on the amplitude of primordial density fluctuations at the horizon crossing epoch (Green et al. 2004). The PBH abundance is expected to be a probe of primordial density fluctuations on small scales which cannot be accessible by CMB or LSS observations.

Constraints on the abundance of PBHs have been studied in many papers and continue to be updated (Carr et al. 2010). PBHs with mass smaller than 10^{15} g have evaporated by the present epoch because the evaporation time scale by Hawking radiation is less than the Hubble time scale today (Hawking 1974). However evaporation of PBHs generates additional entropy in the Universe after inflation (Zel'dovich & Starobinskii 1976), affects on big bang nucleosynthesis (Vainer et al. 1978; Vainer & Naselskii 1978; Miyama & Sato 1978; Zeldovich et al. 1977; Lindley 1980) and distorts the CMB blackbody spectrum (Tashiro & Sugiyama 2008). PBH evaporation may also produce the observable gamma-ray background (Page & Hawking 1976; MacGibbon & Carr 1991). According to measurements of these cosmological phenomena, there are strong constraints on the abundance of PBHs with mass smaller than 10^{15} g.

PBHs with mass larger than 10^{15} g survive in the present Universe. One of the constraints on such PBHs can be set from the fact that the current density parameter of PBHs, Ω_{PBH} , cannot exceed the cold dark matter density parameter observed at the present epoch, Ω_{C} . Conventionally, the constraint on PBH abundance is given by $\beta(M)$ which is the fraction of the regions of mass M collapsing into PBHs at the formation epoch (Carr 1975). The constraint on the density parameter of PBHs today, $\Omega_{\text{PBH}} < \Omega_{\text{C}}$, implies $\beta < 2 \times 10^{-18}(M/10^{15}\text{g})^{1/2}$ from WMAP 7-year data, i.e., $\Omega_{\text{C}} = 0.22$ (Komatsu et al. 2011). Microlensing observations also constrain the abundance of non-evaporating PBHs (Alcock et al. 2001). Ricotti et al.

(2008) have obtained the constraint on PBHs with mass larger than $0.1 M_{\odot}$, investigating the effects of such PBHs on cosmic reionization and CMB temperature anisotropies and distortions. The future gravitational wave observations are also expected to provide a probe of the massive PBH abundance (Ioka et al. 1999; Inoue & Tanaka 2003).

In this paper, we evaluate the 21 cm brightness temperature produced by PBHs and study the potential of 21 cm observations to give the constraint on the abundance of PBHs. Mack & Wesley (2008) have investigated the signatures of evaporating PBHs in 21 cm brightness temperature. Accordingly, they have concentrated on PBHs whose mass range is $5 \times 10^{13} \text{ g} \lesssim M_{\text{PBH}} \lesssim 10^{17} \text{ g}$. On the contrary, here, we focus on non-evaporating PBHs with mass much larger than 10^{15} g . It has been shown that PBHs with large mass could produce X-ray and UV photons through the accretion of matter to PBHs and these photons heat up and ionize intergalactic medium (IGM) (Carr 1981; Gnedin et al. 1995; Miller & Ostriker 2001; Ricotti et al. 2008). The heated and ionized IGM gas may produce the observable deviation of the 21 cm brightness temperature from the background. Our aim in this paper is to evaluate this deviation and to discuss the potential of the 21 cm observation to give the constraint on the non-evaporating PBH abundance.

The paper is organized as follows. In Section 2, using a simple model of X-ray photon flux due to the accretion to a PBH, we evaluate the ionization and temperature profile near a PBH. In section 3, we calculate the spin temperature and the brightness temperature induced by a PBH. In section 4, the angular power spectrum of 21 cm fluctuations due to PBHs are evaluated. Section 5 is devoted to the conclusion. Throughout the paper, we use parameters for a flat Λ CDM model: $h = 0.7$ ($H_0 = h \times 100 \text{ km/s/Mpc}$), $\Omega_B = 0.05$ and $\Omega_M = 0.26$. These parameters are consistent with WMAP results (Komatsu et al. 2011).

2 IONIZATION AND HEATING OF IGM BY A PBH

The accretion disk of a non-evaporating PBH, whose mass is larger than 10^{15} g , can be a source of X-ray photons. For example, the non-evaporating PBHs are one of the candidates for super massive black hole seeds. PBHs whose masses exceed $10^5 M_{\odot}$ cannot be directly formed through gravitational collapse since the time scale of the collapse becomes longer than cosmological time. Accordingly only the accretion after the formation, which induces X-ray photon emission, makes possible to form such massive black holes (Düchting 2004; Khlopov et al. 2005). It is difficult to theoretically predict the accurate X-ray photon spectrum from PBHs, because the X-ray spectrum depends on the detailed condition of the accretion and the environment of PBHs such as the amount of neutral hydrogens. Hence, for simplicity, we assume that the PBH accretion powers a miniquasar with the power-law spectrum of X-ray photons, according to Kuhlen & Madau (2005),

$$F(E) = \mathcal{A} E^{-1} \text{ s}^{-1}, \quad (1)$$

where \mathcal{A} is set as the tenth of the Eddington luminosity. Here we consider the range of the photon energy E from 200 eV to 100 keV since we assume that emitted photons whose energy are lower than 200 eV are immediately absorbed by the surrounding gas of the PBH. Following Zaroubi et al. (2007), we evaluate the ionization and heating of IGM due to massive PBHs in this section.

The number density of photons per unit time per unit area at distance r from the source is given by

$$\mathcal{N}(E; r) = e^{-\tau(E; r)} \frac{\mathcal{A}}{(4\pi r^2)} E^{-1} \text{ cm}^{-2} \text{ s}^{-1}, \quad (2)$$

$$\tau(E; r) = \int_0^r n_H x_H \sigma(E) dr, \quad (3)$$

where x_H is the hydrogen neutral fraction, n_H is the mean number density of hydrogen at a redshift z and $\sigma(E)$ is the absorption cross-section per hydrogen atom. In order to take into account the contribution from helium atoms as well as hydrogen atoms, we adopt the fitting formula by Zdziarski & Svensson (1989),

$$\sigma = 4.25 \times 10^{-21} \left(\frac{E}{250 \text{ eV}} \right)^{-p}, \quad p = \begin{cases} 2.65 & \text{for } E < 250 \text{ eV,} \\ 3.30 & \text{for } E > 250 \text{ eV.} \end{cases} \quad (4)$$

Using the function $\mathcal{N}(E; r)$, we can write the ionization rate per hydrogen atom at the distance r from the source as

$$\Gamma(r) = \int_{E_0}^{\infty} \sigma(E) \mathcal{N}(E; r) \left(1 + \frac{E}{E_0} \phi(E, x_e) \right) \frac{dE}{E}, \quad (5)$$

where the term, $(E/E_0)\phi(E, x_e)$, is introduced to consider the secondary ionization by the photoelectrons produced by energetic photons ($E > 100 \text{ eV}$). We apply the fitting formula of ϕ by Dijkstra et al. (2004) for the low energy region $E < 0.5 \text{ keV}$ and by Shull & van Steenberg (1985) for the high energy region $E > 0.5 \text{ keV}$.

The neutral fraction of hydrogen is obtained by solving the equation of the ionization-recombination equilibrium

$$\alpha_H n_H^2 (1 - x_H)^2 = \Gamma(r) n_H x_H \quad (6)$$

where α_H is the recombination cross-section; $\alpha_{HI} = 2.6 \times 10^{-13} \text{ cm}^3 \text{ s}^{-1}$,

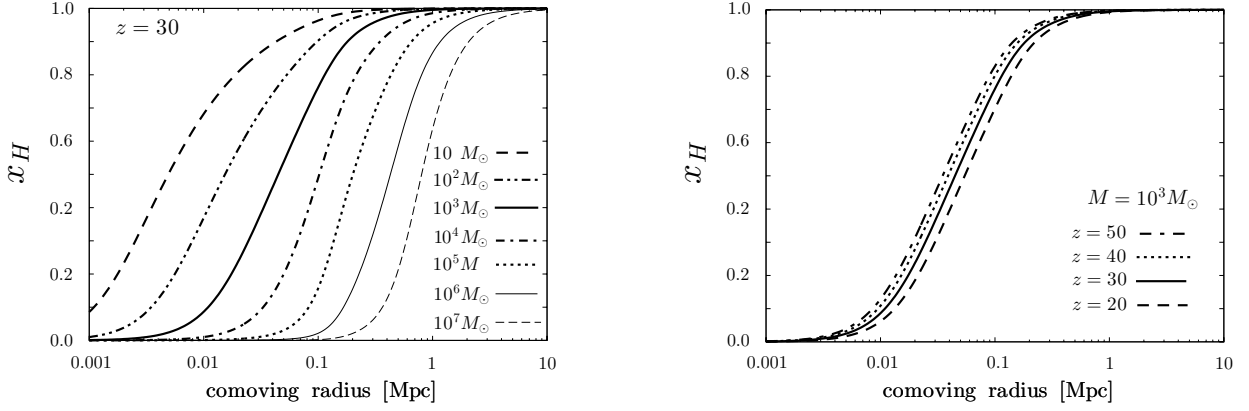


Figure 1. The neutral fraction of hydrogen as a function of comoving distance from the source. The left panel shows the dependence on mass at $z = 30$. The lines represent the neutral fraction with masses ranging from $10 M_\odot$ to $10^7 M_\odot$ from left to right. The right panel shows the dependence on redshift for a PBH with $M = 10^3 M_\odot$. The dotted-dashed, dotted, solid and dashed lines represent the neutral fraction at $z = 50$, $z = 40$, $z = 30$ and $z = 20$, respectively.

Solving Eq. (6), we show the neutral fraction of hydrogen for different masses and for different redshifts in the left and right panels of Fig. 1, respectively. Here we assume that the density around a PBH is same as the mean density of the Universe. The comoving radius of the ionization sphere is made large by massive PBHs. Increasing mass of PBHs means enhancing the ionization photons, because we assume that the flux of the ionization photons is proportional to a tenth of the Eddington luminosity. As the Universe evolves, the comoving radius of the ionization sphere increases slowly.

Next, we evaluate the kinetic temperature of IGM around a PBH. The heating rate per unit volume per unit time at the distance r from the source is obtained by considering the photons absorbed by the IGM at r ,

$$\mathcal{H}(r) = f n_H x_H(r) \int_{E_0}^{\infty} \sigma(E) \mathcal{N}(E; r) dE \quad (7)$$

where f is the fraction of the absorbed photon energy through the collisional excitations of the IGM. Shull & van Steenberg (1985) provided a simple fitting formula $f = C [1 - (1 - x^a)^b]$, where $C = 0.9771$, $a = 0.2663$, $b = 1.3163$ and $x = 1 - x_H$ is the ionized fraction.

The kinetic temperature of the IGM at the distance r , $T_k(r)$, is determined by the balance between the heating and the Compton cooling due to CMB photons.

$$\mathcal{H}(r) = \frac{8\sigma_T}{3m_e} T_\gamma^4 (1 - x_H) (T_k(r) - T_\gamma) + 2HT_k(r), \quad (8)$$

where σ_T is the cross section for the Compton scattering and T_γ is CMB temperature. Here we also take into account the cooling by the expansion of the Universe.

Fig. 2 shows the gas temperature profiles for different masses in the left panel and for different redshifts in the right panel. Here we add the background temperature to the kinetic temperature in order to match both temperatures at a large distance from a PBH. Near the source, the temperature is determined by the heating rate and the Compton cooling rate. With increasing the distance from the source, neutral fraction grows and the optical depth τ becomes larger. Accordingly, the number density of photons damps as shown in Eq. (2). As a result, the temperature starts to decrease rapidly. Because the Compton cooling depends on the number of free electrons, this cooling becomes ineffective at the distance where the neutral fraction of hydrogen becomes almost unity. For example, this scale corresponds to 0.1 comoving Mpc for a PBH with $M = 10^3 M_\odot$ at $z = 30$. Beyond this point, the temperature mildly decreases due to the cooling of the cosmic expansion. The kinetic temperature at the inner side is independent on a PBH mass. However the region of the high temperature becomes larger as the PBH mass increases. In the right panel of Fig. 2, the redshift dependence of the kinetic temperature is shown. The larger the neutral hydrogen density is, the larger the heating efficiency becomes as in Eq. (7). Therefore the heated temperature becomes high as the redshift increases.

3 21 CM BRIGHTNESS TEMPERATURE DUE TO A PBH

As shown in the previous section, a PBH ionizes and heats the surrounding region by the X-ray emissions. These ionization and heating leave an observable signature as the differential brightness temperature of the 21 cm intensity relative to the CMB temperature.

The 21 cm intensity depends on the ratio between the number density of neutral hydrogen in the excitation and ground states in the hyperfine structure. This ratio can be quantified by the spin temperature T_s . The spin temperature is determined

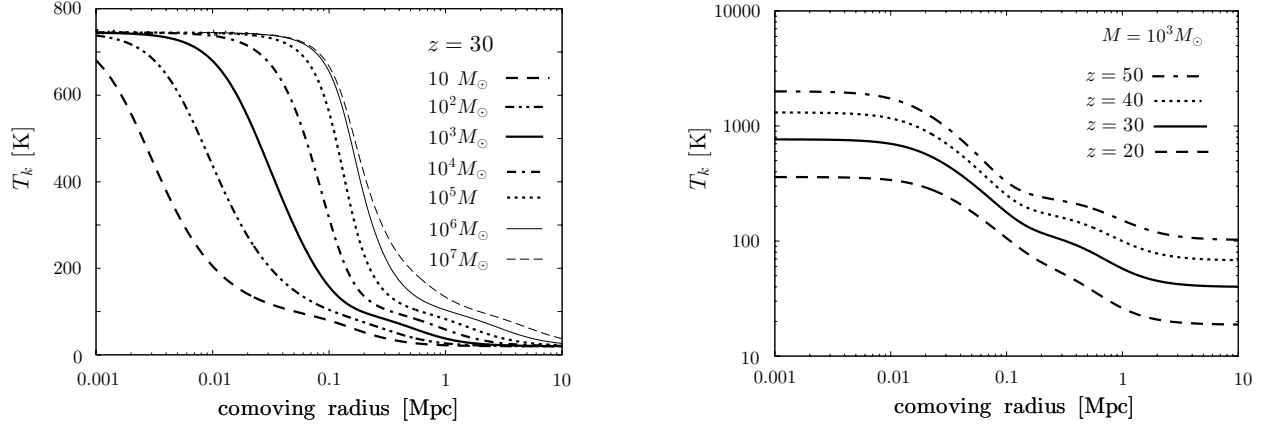


Figure 2. The kinetic temperature of hydrogen gas as the function of the comoving radius. The left panel shows the dependence on a PBH's mass at $z = 30$. The right panel shows the dependence on the redshift for a PBH with $M = 10^3 M_\odot$. In both panels, the representations of lines are same as in Fig. 1.

by the balance between three processes: absorption of CMB photons, collisional excitation in the kinetic temperature T_k , and Lyman α pumping (Wouthuysen 1952; Field 1958). In the steady state approximation between these processes, the spin temperature is obtained by (Field 1958)

$$T_s = \frac{T_* + T_\gamma + y_k T_k + y_\alpha T_k}{1 + y_k + y_\alpha}, \quad (9)$$

where T_* is 0.068 K which is the temperature corresponding to the energy difference between the levels in the hyperfine structure, and y_k and y_α are the kinetic and Lyman- α coupling efficiencies, respectively. The kinetic efficiency is given by

$$y_k = \frac{T_*}{A_{10} T_{kin}} (C_H + C_e + C_p), \quad (10)$$

where A_{10} is the Einstein spontaneous emission rate coefficient, $A_{10} = 2.9 \times 10^{-15} \text{ s}^{-1}$. The terms, C_H , C_e and C_p , represent the de-excitation rates due to neutral hydrogen, electrons and protons, respectively. Here we use the fitting formula by Kuhlen et al. (2006),

$$C_H = n_H \kappa, \quad C_e = n_e \gamma_e, \quad C_p = 3.2 n_p \kappa, \quad (11)$$

where n_e and n_p are the electron and proton number densities, respectively. In Eq. (11), κ is the effective single-atom rate coefficient,

$$\kappa = 3.1 \times 10^{-11} n_H T_k^{0.357} \exp(-32/T_k) \text{ cm}^3 \text{ s}^{-1}, \quad (12)$$

and γ_e is given by $\log(\gamma_e/1 \text{ cm}^3 \text{ s}^{-1}) = -9.607 + 0.5 \log T_k \times \exp(-(\log T_k)^{4.5}/1800)$ for $T_k < 10^4 \text{ K}$ and $\gamma_e = \gamma_e(T_k = 10^4 \text{ K})$ for $T_k > 10^4 \text{ K}$.

The Lyman- α coupling efficiency is given by Field (1958),

$$y_\alpha = \frac{16\pi^2 T_* e^2 f_{12} J_0}{27 A_{10} T_k m_e c}, \quad (13)$$

where $f_{12} = 0.416$ is the oscillator strength of the Lyman α transition, and e and m_e are the electron charge and mass, respectively. In Eq. (13), J_0 is the flux of the Lyman α photons due to collisional excitations. At the distance r from the source, J_0 can be written as (Zaroubi et al. 2007)

$$J_0(r) = \frac{\phi_\alpha c}{4\pi H(z) \nu_\alpha} n_H x_H(r) \int_{E_0}^{\infty} \sigma(E) \mathcal{N}(E; r) \frac{dE}{h\nu_\alpha}, \quad (14)$$

where ϕ_α is the fraction of the absorbed energy going into the collisional excitation of Lyman α . Shull & van Steenberg (1985) gave the following analytical form,

$$\phi_\alpha \approx 0.48 (1 - (1 - x_H)^{0.27})^{1.52}. \quad (15)$$

Now we can calculate the spin temperature in case existing a PBH according to the results in the previous section. We show the results in Fig. 3. The left panel shows the spin temperature for different masses of a PBH at $z = 30$ and the right panel represents the spin temperature for different redshifts for $M = 10^3 M_\odot$.

In the highly ionized region, the profile of the spin temperature is flat and does not depend on PBH's mass as shown in the left panel of Fig. 3. Since it is highly ionized, the spin temperature is determined by the CMB temperature and the term of the kinetic efficiency. As the neutral fraction goes up with increasing the distance, however, the Lyman α efficiency y_α becomes larger so that the term of Lyman α coupling begins to be effective. Peaks of T_s in the small radius for small

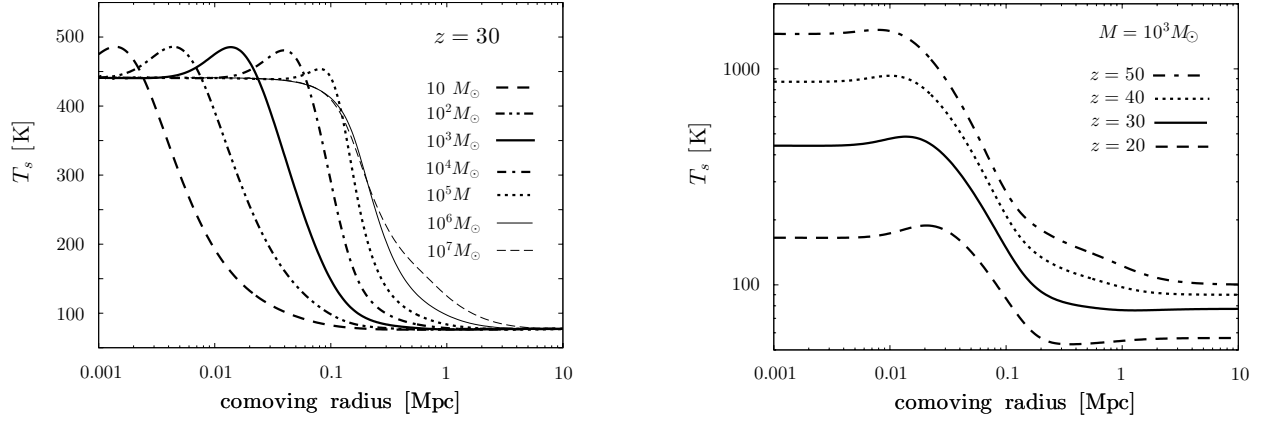


Figure 3. The spin temperature as the function of the comoving radius. The left panel shows the dependence on PBH’s mass at $z = 30$. The right panel shows the dependence on the redshift for a PBH with $M = 10^3 M_\odot$. In both panels, the representations of lines are same as in Fig. 1.

PBH masses shown in the left panel are caused due to this effect. It should note that the peak values are also independent on mass since T_s approaches to T_k for a large value of y_α . Because the flux of Lyman- α quickly decreases as the radius increases, the spin temperature also drops. Finally, the spin temperature settles down to the one determined by the background CMB and kinetic temperatures. The larger the PBH’s mass is, the larger the region where the spin temperature is higher than the background one becomes.

Because the kinetic temperature strongly depends on the redshift as shown in the right panel of Fig. 2, the amplitude of the spin temperature also has the strong dependence on the redshift as shown in the right panel of Fig. 3. The spin temperature is almost same as the kinetic temperature in the ionized region at high redshifts ($z > 40$), since the kinetic efficiency y_k dominates other contributions in Eq. (9). In low redshifts ($z < 30$), we find the region where the spin temperature is lower than the background one at the edge of the heated region. In these redshifts the background spin temperature is almost the CMB temperature, while the background spin temperature is between the CMB and kinetic temperatures in redshifts, $30 < z < 50$. Since the kinetic temperature is lower than the CMB temperature at the edge, the Lyman- α coupling is strong and draws the spin temperature toward the kinetic temperature. Therefore, there exists a region where the spin temperature becomes lower than the background one. This tendency appears even in Zaroubi et al. (2007).

The differential brightness temperature from the CMB temperature for a given spin temperature T_s is obtained by (Ciardi & Madau 2003)

$$\delta T_b = (20 \text{ mK}) (1 + \delta) \left(\frac{x_H}{h} \right) \left(1 - \frac{T_\gamma}{T_s} \right) \left(\frac{\Omega_B h^2}{0.0223} \right) \left[\left(\frac{1+z}{10} \right) \left(\frac{0.24}{\Omega_M} \right) \right]^{1/2}, \quad (16)$$

where δ is the density contrast. Here we assume $\delta = 0$ as mentioned in section 2. In Fig. 4, δT_b is shown as a function of the comoving radial distance from a PBH. The left panel is for different masses of a PBH at $z = 30$ and the right panel is for different redshifts for $M = 10^3 M_\odot$. The δT_b is almost zero near the source, because hydrogen in such regions are totally ionized. As the neutral fraction increases, the brightness temperature also grows. The peak amplitudes of δT_b are independent on the PBH mass for $M < 10^4 M_\odot$. This is because the spin temperature is much larger than the CMB temperature, $T_s \gg T_\gamma$. Accordingly, from Eq. (16), δT_b becomes independent on T_s and only depends on $(1+z)^{1/2}$. This redshift dependence is shown in the right panel of Fig. 4. On the other hand, the peak amplitude becomes smaller for a mass of the PBH higher than $10^5 M_\odot$ in our model.

As in the case of T_s , the region where the differential brightness temperature is below the background value exists near the edge at $z < 30$. Eventually, however, δT_b matches the background value at a large distance. The size of the region where we can detect δT_b becomes larger with increasing mass, and reaches almost 10 Mpc .

4 THE ANGULAR POWER SPECTRUM OF 21 CM BRIGHTNESS TEMPERATURE DUE TO PBHS

In order to study the potential of cosmological 21 cm observations to give a constraint on the PBH abundance, we evaluate the angular power spectrum of 21 cm fluctuations due to PBHs with mass M ,

$$C_\ell(z_{\text{obs}}) = \int dr \frac{W^2(r, r_{\text{obs}})}{r^2} P(\ell/r, r), \quad (17)$$

where z_{obs} is the redshift by choosing the observation frequency $\nu_{\text{obs}} = (1 + z_{\text{obs}})\nu_{21}$ with $\nu_{21} = 1420$. MHz, r is the comoving radial distance, $W(r, r_{\text{obs}})$ is the window function of a 21 cm observation, and $P(k, r)$ is the power spectrum of the brightness

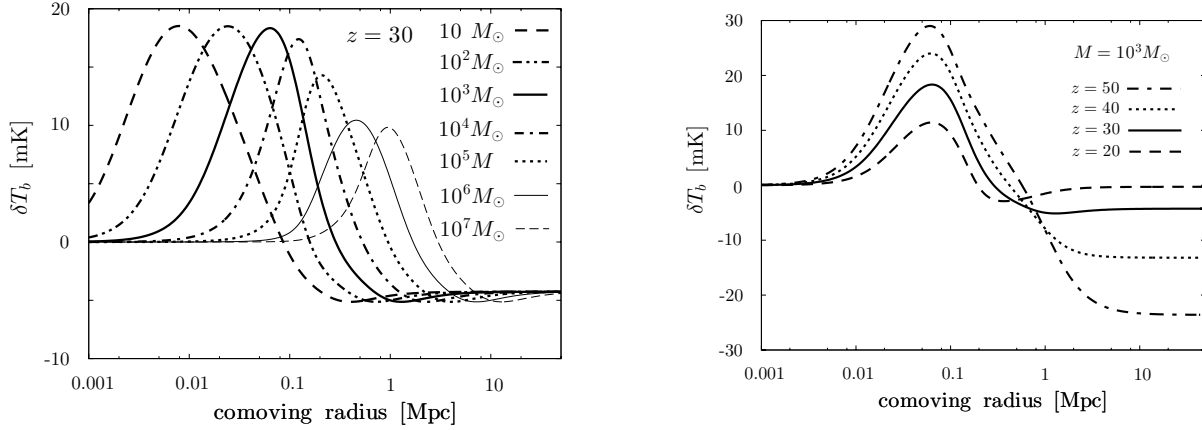


Figure 4. The brightness temperature fluctuations as the function of the comoving radius. The left panel shows the dependence on the PBH’s mass at $z = 30$. The right panel shows the dependence on the redshift for a PBH with $M = 10^3 M_\odot$. In both panels, the representations of lines are same as in Fig. 1.

temperature fluctuations at r . In Eq. (17), since we are only interested in the brightness temperature fluctuations on small scales ($\ell \gg 10$), we employ the Limber approximation.

We obtain the power spectrum of the brightness temperature fluctuations $P(k, r)$ by PBHs with mass M , following the halo formalism (Seljak 2000). We assume that the spacial distribution of PBHs is totally random. Therefore, the power spectrum due to PBHs can be expressed only by the Poisson contribution,

$$P(k) = n_{\text{PBH}}(M) |\Delta T_b^2(k)|^2, \quad (18)$$

where $n_{\text{PBH}}(M)$ is the comoving number density of PBHs with M . The number density of PBHs is described by using the density parameter Ω_{PBH} as

$$n_{\text{PBH}}(M) = \frac{\rho_c \Omega_{\text{PBH}}}{M} = 1.36 \times 10^{-2} \left(\frac{\Omega_{\text{PBH}}}{10^{-9}} \right) \left(\frac{M}{10^4 M_\odot} \right)^{-1} \text{Mpc}^{-3}, \quad (19)$$

where ρ_c is the critical density at the present epoch. In Eq. (18), $\Delta T_b(k)$ is the Fourier transform of the brightness temperature fluctuations from the background value,

$$\Delta T_b(k) = 4\pi \int x^2 dx (\delta T_b(x) - \delta T_{b0}) \frac{\sin(xk)}{xk}, \quad (20)$$

where x is the comoving radius and δT_{b0} is the background brightness temperature given by Eqs. (9) and (16) with the background kinetic temperature, T_{k0} .

Using δT_b obtained in the previous section as shown in Fig. 4, we calculate the angular power spectrum. The results are shown in Fig. 5. Here we set $\Omega_{\text{PBH}} = 10^{-11}$. For simplicity, we assume that the window function has a strong peak at $r = r_{\text{obs}}$ and can be approximated as $W^2(r, r_{\text{obs}}) = \delta(r - r_{\text{obs}})$. Since the promising signal of the cosmological 21 cm fluctuations is one due to the primordial density fluctuations, we also plot the angular power spectrum of those fluctuations obtained through CAMB (Lewis & Challinor 2007).

In the left panel of Fig. 5, it is shown that the peak amplitude of the angular spectrum is independent on PBH’s mass. The peak locations shift toward large scales for massive PBHs. Moreover, the power law index of the spectrum matches the one due to the primordial density fluctuations on small ℓ ’s. The overall amplitude of the spectrum is simply proportional to Ω_{PBH} or the PBH number density. For $\Omega_{\text{PBH}} = 10^{-12}$, it is shown that the angular spectrum of PBHs with mass $10^3 M_\odot$ matches with the one due to the primordial density fluctuations’ one if Ω_{PBH} is smaller (larger). To match these two spectra, we find the critical value of Ω_{PBH} as $\Omega_{\text{PBHc}} \equiv 10^{-12} (M/10^3 M_\odot)^{-0.2}$ for $z = 30$. The PBH spectrum dominates over the one due to the primordial density fluctuations if Ω_{PBH} exceeds Ω_{PBHc} .

The right panel of Fig. 5 shows that, although the peak location does not depend on the redshift, the redshift dependence of the peak amplitude is different from that due to the primordial density fluctuations. As the result, while the PBH contribution for Ω_{PBHc} is subdominant at $z = 40$, even the PBHs with roughly $0.1 \times \Omega_{\text{PBHc}}$ can produce the spectrum comparable with that due to the primordial density fluctuations at $z = 20$.

The brightness temperature profile at lower redshifts, $z < 30$, has both positive and negative peaks as shown in Fig. 4. The reason to have a negative peak is because there exists the region where the brightness temperature is lower than the background, which is rather difficult to see in the figure. Accordingly, the angular power spectrum due to PBHs also has two peaks at $z < 30$ as shown in Fig. 5. The peak on a larger scale is due to the negative peak of ΔT_b , while that on a small scale is due to the positive one.

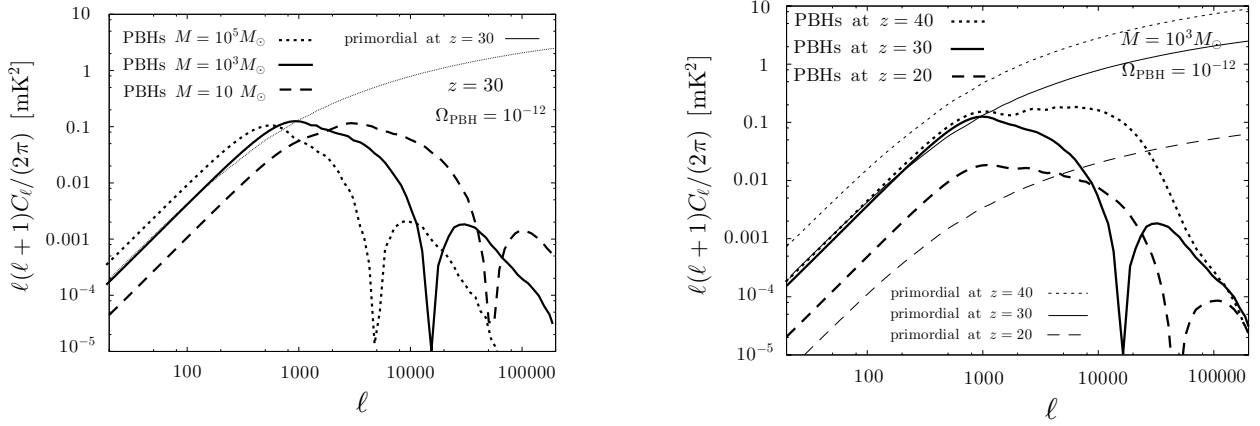


Figure 5. The angular power spectrum of 21 cm brightness temperature fluctuations produced by PBHs. comoving radius. The left panel shows the dependence on the PBH mass at $z = 30$. The dotted, solid and dashed lines represent for PBHs with $M = 10^5 M_\odot$, $10^3 M_\odot$ and $10 M_\odot$, respectively. The right panel shows the dependence on the redshift for PBHs with $M = 10^3 M_\odot$. The dotted, solid and dashed lines are for PBHs at $z = 40$, $z = 30$ and $z = 20$, respectively. We assume $\Omega_{\text{PBH}} = 10^{-12}$ in both panels. For comparison, we also plot the angular power spectrum due to the primordial density fluctuations as thin lines.

At the last of this section, we discuss the constraint by a future observation such as the square kilometer array (SKA)-like interferometer. The noise power spectrum of an observation including the beam effects is given by (Knox 1995)

$$\frac{\ell(\ell+1)}{2\pi} N_\ell^{21} = \frac{\ell(\ell+1)}{t_{\text{obs}} \Delta\nu} \left(\frac{D \lambda T_{\text{sys}}}{A_{\text{eff}}} \right)^2 \exp \left[\frac{\ell(\ell+1)}{\ell_b^2} \right], \quad (21)$$

where $A_{\text{eff}}/T_{\text{sys}}$ is the sensitivity (an effective area divided by the system temperature), t_{obs} is the observation time, $\Delta\nu$ is the frequency bandwidth, D is the length of the baseline and ℓ_b is given by $\ell_b = 4\sqrt{\ln 2}/\theta_{f_w}$ with the resolution $\theta_{f_w} \sim \lambda/D$. Here we adopt the current design of SKA¹; $A_{\text{eff}}/T_{\text{sys}} = 2000 \text{ m}^2\text{K}^{-1}$, $t_{\text{obs}} = 1000$ hour, $\Delta\nu = 1$ MHz and $D = 5$ km. In this design, the noise power spectrum is evaluated as

$$\frac{\ell(\ell+1)}{2\pi} N_\ell^{21} \sim 73 \text{ mK}^2 \left(\frac{\ell}{1000} \right)^2 \left(\frac{1+z}{30} \right)^2 \exp \left[\left(\frac{\ell}{2500} \frac{z+1}{30} \right)^2 \right]. \quad (22)$$

The noise power spectrum exponentially grows on larger multipoles than $\ell_b = 2500(30/(1+z))$. The amplitude of the angular power spectrum due to the PBHs is scaled by Ω_{PBH} . Accordingly we find that, in order to overdominate the noise spectrum, $\Omega_{\text{PBH}} \sim 10^{-9}(M/10^3 M_\odot)^{-0.2}$ is required for $M > 10 M_\odot$ at $z = 30$ and $\Omega_{\text{PBH}} \sim 10^{-10}(M/10^3 M_\odot)^{-0.2}$ is for $M > 10 M_\odot$ at $z = 20$. Since the angular spectrum due to PBHs with mass less than $10 M_\odot$ has a peak on larger multipoles than ℓ_b in the SKA design, there is no opportunity to measure the anisotropy spectrum due to such small mass PBHs by SKA.

5 CONCLUSION

We have investigated the 21 cm signal produced by massive PBHs whose masses are larger than $10 M_\odot$. Assuming the power-law spectrum of X-ray photons from an accretion disk, we have studied the ionization and heating of IGM gas near a PBH and evaluated the differential 21 cm brightness temperature. We have shown that a PBH can induce an observable signal of differential 21 cm brightness temperature. The size of the region where we can find the differential brightness temperature typically reaches 1–10 Mpc for our interested PBH mass range while the size depends on the PBH mass.

We have also calculated the angular power spectrum of 21 cm fluctuations due to PBHs. The peak position of the angular spectrum depends on the PBH mass, while the amplitude is independent. Comparing it with the angular power spectrum caused by primordial density fluctuations, we have found that both of them become comparable if $\Omega_{\text{PBH}} = 10^{-12}(M/10^3 M_\odot)^{-0.2}$ at $z = 30$ and $10^{-13}(M/10^3 M_\odot)^{-0.2}$ at $z = 20$ for PBH's mass from $10 M_\odot$ to $10^8 M_\odot$. If the density parameter is larger than these values, the angular power spectrum due to PBHs exceeds the one from primordial fluctuations and can be measured. In other words, we cannot set constraints on the PBH density parameter below these values from 21 cm observations. If we consider the sensitivity of the SKA-like observation, for example, we can detect the signal of PBHs up to $\Omega_{\text{PBH}} = 10^{-9}(M/10^3 M_\odot)^{-0.2}$ at $z = 30$ and $10^{-10}(M/10^3 M_\odot)^{-0.2}$ at $z = 20$ for PBHs with mass from $10^2 M_\odot$ to $10^8 M_\odot$.

The ionization of IGM due to PBHs with such density parameters does not affect the global reionization history of

¹ <http://www.skatelescope.org/>

the universe since reionization from each PBH only covers a tiny patch of the universe. Unlike reionization from first stars, therefore, such reionization has little impact on CMB temperature anisotropies. Accordingly the PBH density parameter constrained from WMAP data, that is $\Omega_{\text{PBH}} < 10^{-7}$ (Ricotti et al. 2008), is several order of magnitude larger than the value we obtained above. In other words, we can conclude that 21 cm fluctuation observations have a potential to probe the PBH abundance which is impossible to access by CMB observations.

The most theoretical uncertainty in this model is the flux of photons due to the accretion to PBHs. In this paper, we assume that the X-ray photon flux amplitude is a tenth of the Eddington luminosity for simplicity. The luminosity is considered to depend on the matter accretion rate to a PBH. Ricotti et al. (2008) have studied the luminosity for the Bondi-Hoyle accretion in details. Although the luminosity depends on the PBH mass and feedback effect on the ionization and temperature, they have shown that the luminosity for a PBH with $M = 10^3 M_{\odot}$ is roughly a hundredth of the Eddington luminosity at $z > 20$. In our model, the brightness temperature profile near a PBH at a certain redshift depends on only PBH's mass and the amplitude of the angular power spectrum is scaled by Ω_{PBH} . Therefore, if we assume that the amplitude of the X-ray photon flux is a hundredth of the Eddington luminosity, $\Omega_{\text{PBH}c}$, which is the required density parameter for PBHs to dominate the 21 cm fluctuations due to primordial density fluctuations, is $10^{-11}(M/10^4 M_{\odot})^{-0.2}$ at $z = 30$ and $10^{-12}(M/10^4 M_{\odot})^{-0.2}$ at $z = 20$ for PBH's mass from $10 M_{\odot}$ to $10^8 M_{\odot}$.

ACKNOWLEDGMENTS

H. T. is supported by the DOE. N. S. is supported by Grand-in-Aid for Scientific Research No. 22340056. This research has also been supported in part by World Premier International Research Center Initiative, MEXT, Japan.

REFERENCES

- Alcock C., et al. 2001, *Astrophys. J. Lett.*, 550, L169
 Carr B. J., 1975, *Astrophys. J.*, 201, 1
 Carr B. J., 1981, *MNRAS*, 194, 639
 Carr B. J., Hawking S. W., 1974, *MNRAS*, 168, 399
 Carr B. J., Kohri K., Sendouda Y., Yokoyama J., 2010, *Phys. Rev. D*, 81, 104019
 Ciardi B., Madau P., 2003, *Astrophys. J.*, 596, 1
 Dijkstra M., Haiman Z., Loeb A., 2004, *Astrophys. J.*, 613, 646
 Düchting N., 2004, *Phys. Rev. D*, 70, 064015
 Field G. B., 1958, *Proc. IRE*, 46, 240
 Gnedin N. Y., Ostriker J. P., Rees M. J., 1995, *Astrophys. J.*, 438, 40
 Green A. M., Liddle A. R., Malik K. A., Sasaki M., 2004, *Phys. Rev. D*, 70, 041502
 Hawking S. W., 1974, *Nature*, 248, 30
 Inoue K. T., Tanaka T., 2003, *Physical Review Letters*, 91, 021101
 Ioka K., Tanaka T., Nakamura T., 1999, *Phys. Rev. D*, 60, 083512
 Khlopov M. Y., Rubin S. G., Sakharov A. S., 2005, *Astroparticle Physics*, 23, 265
 Knox L., 1995, *Phys. Rev. D*, 52, 4307
 Komatsu E., et al. 2011, *Astrophys. J. Suppl.*, 192, 18
 Kuhlen M., Madau P., 2005, *MNRAS*, 363, 1069
 Kuhlen M., Madau P., Montgomery R., 2006, *Astrophys. J. Lett.*, 637, L1
 Lewis A., Challinor A., 2007, *Phys. Rev. D*, 76, 083005
 Lindley D., 1980, *MNRAS*, 193, 593
 MacGibbon J. H., Carr B. J., 1991, *Astrophys. J.*, 371, 447
 Mack K. J., Wesley D. H., 2008, arXiv:0805.1531
 Miller M. C., Ostriker E. C., 2001, *Astrophys. J.*, 561, 496
 Miyama S., Sato K., 1978, *Progress of Theoretical Physics*, 59, 1012
 Page D. N., Hawking S. W., 1976, *Astrophys. J.*, 206, 1
 Ricotti M., Ostriker J. P., Mack K. J., 2008, *Astrophys. J.*, 680, 829
 Seljak U., 2000, *MNRAS*, 318, 203
 Shull J. M., van Steenberg M. E., 1985, *Astrophys. J.*, 298, 268
 Tashiro H., Sugiyama N., 2008, *Phys. Rev. D*, 78, 023004
 Vainer B. V., Dryzhakova O. V., Naselskii P. D., 1978, *Soviet Astronomy Letters*, 4, 185 [1978, *Pis ma Astronomicheskii Zhurnal*, 4, 344]
 Vainer B. V., Naselskii P. D., 1978, *Soviet Astronomy*, 22, 138 [1978, *Astronomicheskii Zhurnal*, 55, 231]

Wouthuysen S. A., 1952, *Astronomical Journal*, 57, 31

Zaroubi S., Thomas R. M., Sugiyama N., Silk J., 2007, *MNRAS*, 375, 1269

Zdziarski A. A., Svensson R., 1989, *Astrophys. J.*, 344, 551

Zeldovich I. B., Starobinskii A. A., Khlopov M. I., Chechetkin V. M., 1977, *Soviet Astronomy Letters*, 3, 110 [1977, *Pis ma Astronomicheskii Zhurnal*, 3, 208]

Zel'dovich Y. B., Starobinskii A. A., 1976, *Soviet Journal of Experimental and Theoretical Physics Letters*, 24, 571 [1976, *ZhETF Pis ma Redaktsiiu*, 24, 616]